J. Wind Eng. Ind. Aerodyn. 147 (2015) 43–57

Contents lists available at ScienceDirect

Journal of Wind Engineering and Industrial Aerodynamics

journal homepage: www.elsevier.com/locate/jweia

CFD simulation of wind flow over natural complex terrain: Case study with validation by field measurements for Ria de Ferrol, Galicia, Spain

Bert Blocken [a,b,*], Arne van der Hout [c], Johan Dekker [d], Otto Weiler [c]

[a] Building Physics and Services, Eindhoven University of Technology, P.O. box 513, 5600 MB Eindhoven, The Netherlands
[b] Building Physics Section, Department of Civil Engineering, Leuven University, Kasteelpark Arenberg 40 – bus 2447, 3001 Leuven, Belgium
[c] Deltares, Rotterdamseweg 185, P.O. Box 177, 2600 MH Delft, The Netherlands
[d] Maritime Research Institute Netherlands (MARIN), P.O. Box 28, 6700 AA Wageningen, The Netherlands

ARTICLE INFO

Article history:
Received 24 December 2014
Received in revised form
20 September 2015
Accepted 20 September 2015

Keywords:
Computational Fluid Dynamics (CFD)
Wind flow
Complex terrain
Micro-scale topography
Heterogeneous rough terrain
Surface roughness
Succession of hills
Harbour engineering
Experimental validation

ABSTRACT

Accurate and reliable Computational Fluid Dynamics (CFD) simulations of wind flow over natural complex terrain are important for a wide range of applications including dispersion of pollutants, wind energy resource assessment and ship manoeuvring in channels and near harbours. In the past 50 years, a very large number of CFD studies of wind flow over hills have been performed. However, a detailed review of the literature shows a lack of CFD studies including validation by field measurements for natural complex terrain beyond the case of isolated hills. Therefore, this paper presents a CFD study with field measurement validation for natural complex terrain that consists of an irregular succession of hills and valleys surrounding a narrow entrance channel. The aim of the study is twofold: (1) to evaluate the accuracy of 3D steady Reynolds-averaged Navier–Stokes (RANS) simulations with a revised k–ε model for calculating mean wind-velocity patterns over this type of natural complex terrain; and (2) to provide mean velocity data that can be used as input for real-time ship manoeuvring simulations to evaluate accessing the LNG terminal with larger LNG carriers. The irregular hilly terrain is expected to yield complex wind environmental conditions in the channel and complex forces on the LNG carriers. The study focuses on high wind speed conditions, for which the atmospheric boundary layer exhibits neutral stratification. The simulations are performed with 3D steady RANS and the realisable k–ε model for 12 wind directions. Special attention is given to surface roughness parameterisation and specification. The simulation results of mean wind speed and wind direction are generally within 10–20% of the corresponding measurement values. The results show that for wind directions 60° and 90°, the funnelling effect leads to an increase of wind speed in the channel compared to the wind speed over open sea. For other wind directions, the topography leads to a reduction of the wind speed in the channel, but also to strong wind speed gradients along the channel axis, which are important for ship manoeuvring. The study shows that for the present application, the 3D steady RANS approach with the realisable k–ε model can provide an accurate assessment of the complex mean wind-flow patterns and the funnelling effect by the natural complex topography on the wind.

1. Introduction

The study of wind flow over hills, valleys and other types of complex topography is important for many wind engineering applications, including dispersion of pollutants (e.g. Dawson et al. (1991), Apsley and Castro (1997a, 1997b), Ohba et al. (2002)), wind energy resource assessment (e.g. Taylor and Teunissen (1987), Palma et al. (2008), Conan et al. (2012), Chaudhari (2014)) and ship manoeuvring in harbours. This type of flows can be studied by field experiments, reduced-scale wind-tunnel measurements or numerical simulation with Computational Fluid Dynamics (CFD).

In the past 50 years, Computational Fluid Dynamics (CFD) has increasingly been developed and applied as a powerful assessment tool in wind engineering (Blocken, 2014). This is demonstrated by both general review papers (e.g. Murakami (1993, 1997, 1998), Murakami et al. (1999), Stathopoulos (1997, 2002), Baker (2007), Blocken et al. (2011), Moonen et al. (2012), Meroney and Derickson (2014), Blocken (2014, 2015)) and review papers on topics of particular interest, such as dispersion of pollutants (e.g. Meroney (2004), Canepa (2004), Tominaga and Stathopoulos (2007, 2013), Di Sabatino et al. (2013), Blocken et al. (2013)), natural ventilation

* Corresponding author at: Building Physics and Services, Eindhoven University of Technology, P.O.Box 513, 5600 MB Eindhoven, The Netherlands. Tel.: +31 40 247 2138; fax: +31 40 243 8595.
E-mail address: b.j.e.blocken@tue.nl (B. Blocken).

http://dx.doi.org/10.1016/j.jweia.2015.09.007
0167-6105/

of buildings (e.g. Reichrath and Davies (2002), Norton et al. (2007), Jiru and Bitsuamlak (2010), Ramponi and Blocken (2012)), pedestrian-level wind conditions (e.g. Stathopoulos (2006), Mochida and Lun (2008), Blocken et al. (2012), Blocken and Stathopoulos (2013)), wind-driven rain (e.g. Blocken and Carmeliet (2004, 2010)), snow drift (e.g. Tominaga et al. (2011)), urban thermal environment (e.g. Toparlar et al. (2015)), wind energy resource assessment (e.g. Porté-Agel et al. (2011), Sanderse et al. (2011), Metha et al. (2014)) and wind flow over complex topography (e.g. Wood (2000), Bitsuamlak et al. (2004, 2006)).

CFD has some important advantages compared to field measurements and reduced-scale wind-tunnel testing. The main advantage of field measurements is that they are able to capture the real complexity of the problem under study. Important disadvantages however are that they are not fully controllable due to – among others – the inherently variable meteorological conditions, that they are not possible in the design stage of a building or urban area in the complex terrain and that usually only point measurements are performed. Also wind-tunnel measurements are generally only performed at a few selected points in the model area, and do not provide a whole image of the flow field. CFD on the other hand provides whole-flow field data, i.e. data on the relevant parameters in all points of the computational domain. Unlike reduced-scale wind-tunnel testing, CFD does not suffer from potential violation of similarity requirements because simulations can be conducted at full scale. This is particularly important for studies involving very extensive topographic areas, which is the topic of this paper. A review of both the advantages and disadvantages of wind-tunnel testing for simulating flow over complex terrain was provided by Meroney (1990). Main disadvantages of CFD however are its large sensitivity to the wide range of computational parameters involved – and to the user of the CFD software – and the associated concerns for accuracy and reliability of CFD results. Therefore, CFD verification and validation are imperative, and for this purpose, extensive sets of best practice guidelines for CFD in wind engineering have been developed in the past 15 years (e.g. Casey and Wintergerste (2000), Franke et al. (2004, 2007, 2011), Britter and Schatzmann (2007), Tominaga et al. (2008), Blocken and Gualtieri (2012), Blocken (2015)). It should be noted that validation requires high-quality experimental data, either wind-tunnel data or field data, and these data in turn need to satisfy certain quality criteria (Schatzmann et al., 1997; Schatzmann and Leitl, 2011).

In the past 50 years, a very large number of valuable CFD studies of wind flow over hills have been performed. Initially these studies were based on linearization of the equations of motion. This type of linear CFD models is less computationally demanding and can show good performance for wind flow in absence of flow separation, i.e. for low slopes (e.g. slopes below 10°) (e.g. Hino (1968), Taylor and Gent (1974), Jackson and Hunt (1975), Mason and Sykes (1979), Walmsley et al. (1982), Taylor et al. (1983)). However, later approaches were based on the nonlinear equations of motion (e.g. Raithby et al. (1987)), which are more suitable for cases with flow separation, as flow separation is a process that involves dominant non-linear mechanisms. Most of these nonlinear studies, published in the past 30 years, focused on 2D or 3D generic/idealised isolated hills or sometimes on successions of idealised hills, often with validation by reduced-scale wind-tunnel measurements. Several others were nonlinear CFD studies without specific validation efforts. In addition to linearised models, there have been a variety of simplified but nonlinear CFD models developed to predict flow and dispersion over obstacles, hills and complex terrain features. These usually involved integration of the equations of motion such that the final relations are 1 or 2 dimensional which permits the fast CFD simulation of flow fields (Lee and Meroney, 1988; Meroney, 2012). Finally, in the meteorological community, nonlinear CFD has been used extensively in the past decades to predict flows over complex terrain at the mesoscale. More recently, efforts have been made on integration of mesoscale and microscale modelling (e.g. Schlünzen et al. (2011), Mochida et al. (2011), Yamada and Koike (2011)).

As opposed to these studies, the present paper focuses on nonlinear microscale 3D CFD studies for natural complex terrain including validation with field measurements. The focus on natural complex terrain is driven by the focus of this paper on a practical wind engineering application. And while wind-tunnel measurements can be very suitable for validation, the only real test for practical applications is a comparison with field data. These should be acquired over a sufficiently long time period because of the intrinsic variability of meteorological conditions (Schatzmann and Leitl, 2011). Because of this focus, the next section presents a brief summary of a detailed literature review on CFD studies for wind flow over natural complex terrain including validation with field measurements. This literature review shows that there are many such studies for isolated hills, which are very valuable, but that there is a strong lack of such studies beyond the case of isolated hills. Therefore, this paper in particular presents a CFD study with field measurement validation for a natural complex terrain that consists of an irregular succession of hills and valleys surrounding a narrow entrance channel, i.e. the Ria de Ferrol in Galicia, Spain.

The contents of this paper are as follows. Section 2 presents a brief summary of the literature review together with a short discussion on LES versus steady RANS for complex terrain. In Section 3, the case study problem statement and topography are described. Section 4 addresses the field measurement campaign that was especially made for CFD validation. In Section 5, the computational settings and parameters for the CFD analysis are outlined. The simulation results are presented in Section 6. Section 7 (discussion) and Section 8 (conclusions) conclude the paper.

2. Brief overview of nonlinear CFD studies validated with field measurements

2.1. Case studies for isolated hills

A first set of such studies concern the CFD simulations of wind flow over the Askervein hill (Fig. 1a). The Askervein hill is a relatively isolated low hill of 116 m height near the coast of South Uist in Scotland. It is roughly elliptical in plan form with a 2 km major axis and a 1 km minor axis. A major field campaign to study mostly neutrally-stable boundary-layer flow over the Askervein hill was performed in 1982 and 1983 (Taylor and Teunissen, 1983, 1985, 1987). Raithby et al. (1987) applied the 3D steady RANS equations with the standard k–ε model by Launder and Spalding (1974), however with $C_\mu = 0.033$ instead of the commonly used value 0.09. CFD simulations and experiments of fractional speed-up ratio ΔS, turbulent kinetic energy and turbulent stresses were compared along different transects. For the less steep transect, excellent agreement for ΔS was found at every position along this transect. For the steeper transect, a very close agreement was found for ΔS on the windward side of the hill, with a less close agreement (overestimation by CFD) on the leeward side. Application of a linear model however showed much larger CFD overestimations of ΔS in the lee of the hill. Deviations in turbulent kinetic energy were found for the steep transect in the lee of the hill, at the positions where the mean velocity (and ΔS) was overestimated. Raithby et al. (1987) mentioned that this could be attributed due to intermittent flow separation, which cannot be predicted by the steady RANS CFD approach. In fact, the CFD simulations did predict the flow separation in the lee of the hill, albeit with some discrepancies. Later 3D steady RANS simulations

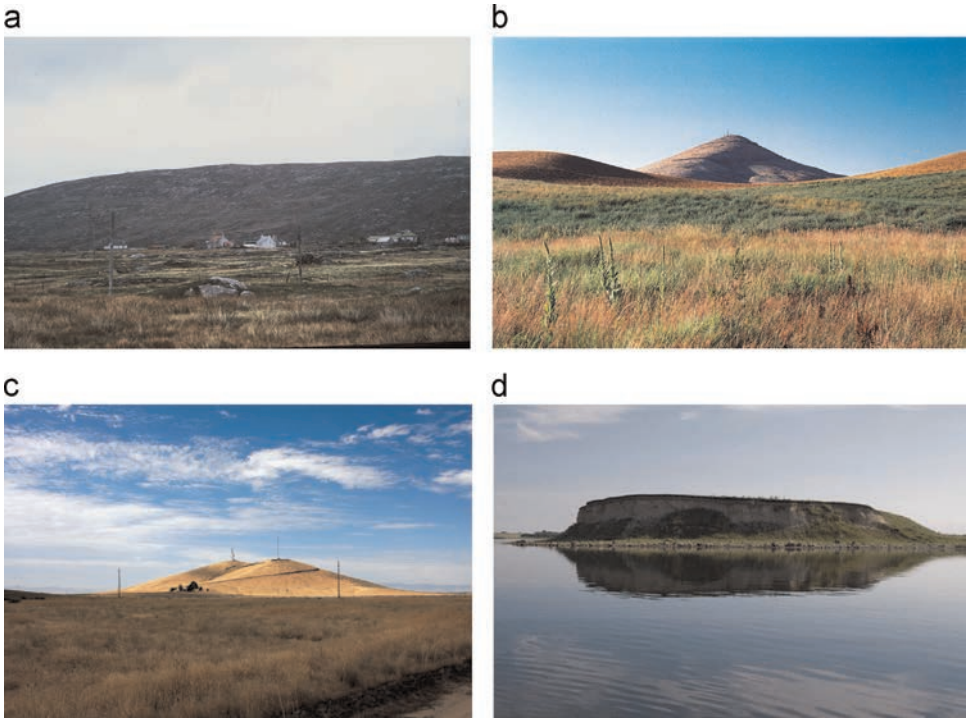

Fig. 1. Perspective views of (a) Askervein hill, Scotland (www.yorku.ca). (b) Steptoe Butte, Washington, USA (CC0 1.0). (c) Cinder Cone Butte, Idaho, USA (kanalawson.com). (d) Bolund hill, Denmark (www.bolund.vindenergi.dtu.dk).

for the Askervein hill were made by – among others – Kim et al. (2000), Prospathopoulos and Voutsinas (2006), Undheim et al. (2006), Balogh et al. (2012) and Moreira et al. (2012), while both steady and unsteady RANS simulations were made by Castro et al. (2003), hybrid RANS/LES by Bechmann and Sorensen (2010) and LES simulations by Silva Lopes et al. (2007).

A second set are the CFD simulations of wind flow and dispersion over Steptoe Butte (Fig. 1b). Steptoe Butte is an isolated 300 m high, approximately axisymmetric conical hill in Whitman Country, Washington, USA (Ryan et al., 1984). The base diameter is about 3400 m. Tracer-gas field measurements were conducted during May and June 1981, with upper-air meteorological data also being recorded. The tracer-gas field experiments indicated advection and/or diffusion of plumes from upwind emission release points into the leeward recirculation zone behind Steptoe Butte, resulting in maximum ground-level concentration on the leeside of the hill (Ryan et al., 1984). 3D steady RANS equations for neutrally-stratified wind flow were performed by Dawson et al. (1991). For closure, the k–ε model with the two modifications by Detering and Etling (1985) was applied. The first modification refers to reducing C_μ from 0.09 to 0.033, while the second refers to reducing ε relative to production with height. The CFD simulations successfully reproduced the presence of the large recirculation zone on the lee slope and its effect on tracer-gas accumulation on the lee slope.

A third set concerns the CFD simulations of wind flow over Cinder Cone Butte (Fig. 1c). Cinder Cone Butte is an isolated, roughly axisymmetric hill of 100 m height and 500 m radius in Idaho, USA. The experimental campaign in 1980 consisted of tracer-gas studies during night-time focused on providing data for strongly stratified flow over complex terrain (Lavery et al., 1982). 3D steady RANS simulations with the limited-length-scale k–ε model (Apsley, 1995; Apsley and Castro, 1997c) were performed by Apsley and Castro (1997a, 1997b). Qualitative flow features such as the separated flow region in the wake and the large horizontal divergence at low level were successfully reproduced in the CFD simulations. Disagreements between simulations and measurements for the – much more complex – gas concentration distributions were clearly attributed to wind veering in combination with the very large sensitivity of ground-level concentrations to approach-flow wind direction.

A fourth set are the CFD simulations of wind flow over the Bolund hill (Fig. 1d). The Bolund hill is a low hill (12 m) in Denmark, surrounded by water with a long uniform fetch, and with a vertical escarpment with a 90° crest. It is 130 m long and 75 m wide. With its steep slopes and cliffs, it is substantially different in geometry than the Askervein hill, Steptoe Butte and Cinder Cone Butte. The Bolund hill surface is uniformly covered by grass. Field measurements of wind speed were performed during a 3-month period in 2007 and 2008 (Bechmann et al., 2009; Berg et al., 2011). Bechmann et al. (2011) report a blind comparison test of micro-scale flow models focused on reproducing the wind flow over the Bolund hill. 57 results were submitted from all branches of the wind energy industry. 3D RANS with the k–ε turbulence model was the most commonly used model (24 submissions) versus only 6 labelled as LES. Surprisingly, RANS with the k–ε turbulence model outperformed all other models. Even the LES results showed much larger speed-up errors than the RANS models with two-equation closure. Note that 3D steady RANS for the Bolund hill was also performed by Prospathopoulos et al. (2012), while LES for the Bolund hill was also performed by Diebold et al. (2013) and Chaudhari (2014), where the latter did manage to correctly predict the flow separation at the windward top edge – which unmistakably has to occur at this sharp edge.

As additional sets, the 3D CFD simulations over the Blashaval hill (Hewer, 1998), Kettles hill (Kim et al., 2000) and the Madeira coastal cliff (Palma et al., 2008) can be mentioned. Note that all of the above-mentioned studies concern hill or valley geometries that, at least for some wind directions, give rise to flow separation.

Because previous studies were mostly performed with RANS, because several more recent studies were also performed with LES and because the case study in the present paper is performed with RANS, the next subsection briefly focuses on LES versus RANS.

2.2. LES versus RANS for wind flow over complex terrain

LES is intrinsically superior in terms of physical modelling to both steady and unsteady RANS. Its theory is well developed and very suitable for simulating the turbulent and non-linear nature of wind flow over complex terrain (Wood, 2000). In addition, its application is increasingly supported by ever increasing computing resources. However, for wind flow modelling over complex terrain, 3D steady RANS remains the main CFD approach up to the present day, where it is often being applied with a satisfactory degree of success. This statement also holds for many other topics in (mainly environmental) wind engineering, such as pedestrian-level wind conditions, natural ventilation of buildings, wind-driven rain, and others, as shown by a detailed review of the literature in computational wind engineering (Blocken, 2014). To the opinion of the present authors, two main reasons are responsible for this: (1) the computational cost of LES. This cost is at least an order of magnitude larger than for RANS, and possibly two orders of magnitude larger when including the necessary actions for verification and validation; (2) the lack of quality assessment in practical applications of LES and the lack of best practice guidelines in LES, which might even lead to a lack of confidence in LES. These arguments are further explained below.

Even without the necessary actions for verification and validation, LES remains very computationally demanding (Wood, 2000). And often too computationally demanding for practical applications, where generally simulations need to be made for at least 12 wind directions (Yoshie et al., 2007), and sometimes even more. When the necessary actions of quality assurance are included – as they should – simulations for several of these different wind directions should be performed on different grids and with different subgrid-scale models to ensure the accuracy and reliability of the simulations. This can be done using techniques such as the Systematic Grid and Model Variation technique (e.g. Klein (2005), Celik et al. (2009), Gousseau et al. (2013)). This care for accuracy and reliability is especially important in LES because, as stated by Hanna (1989)"*… as the model formulation increases in complexity, the likelihood of degrading the model's performance due to input data and model parameter uncertainty increases as well.*" This motivates the establishment of generally accepted extensive best practice guideline documents for LES in wind engineering. However, while such guidelines have been developed for RANS in the past 15 years (e.g. Casey and Wintergerste (2000), Franke et al. (2004, 2007, 2011), Britter and Schatzmann (2007), Tominaga et al. (2008), Schatzmann and Leitl (2011), Blocken and Gualtieri (2012)), this is not the case for LES. This is turn is caused by the computational expense of LES, as the establishment of such guidelines requires extensive sensitivity tests.

Because of the lack of CFD studies validated with field measurements for natural complex terrain beyond the case of the isolated hill and because of the above statements on RANS versus LES, this paper addresses the need for RANS simulations with field measurement validation for natural complex terrain consisting of an irregular succession of hills and valleys.

3. Case study problem statement and topography

The case under study is Ria de Ferrol in Galicia, Spain. It is an entrance channel that connects the LNG terminal of Reganosa in

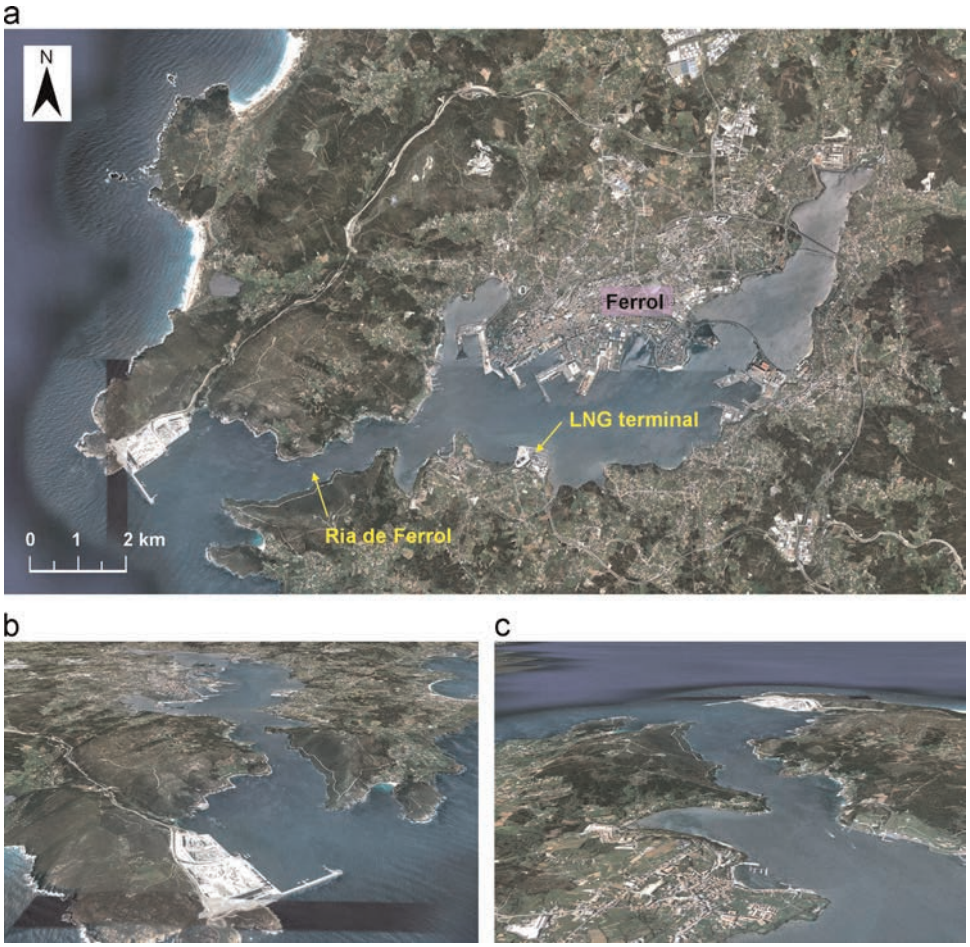

Fig. 2. (a) Top view of Ria de Ferrol and surroundings, with indication of LNG terminal and Ferrol city centre. (b) Perspective view from west. (c) Perspective view from east.

Mugardos with the sea (Fig. 2). It roughly extends from UTM (29 T 553955 E – 4811241.48 N) to (29 T 563337 E – 4813138 N). The immediate surroundings consist of irregular hilly terrain with peak altitudes up to about 250 m both north and south of the Ria. The hilly character is illustrated in Fig. 2b and c, which are perspective views from west and from east, and in Fig. 3a and b, which are perspective views from south.

The aim of the study is twofold: (1) to evaluate the accuracy of 3D steady RANS simulations with a revised k–ε model for calculating mean wind-velocity patterns over this type of natural complex terrain; and (2) to provide mean wind velocity data that can be used as input for real-time manoeuvring simulations to evaluate accessing the LNG terminal with larger LNG carriers. Concerning the first aim, special care is given to high-quality grid generation, to correct implementation of surface roughness parameterisations and roughness transitions – which previous studies have shown to be particularly critical – and to validation with 4 weeks of field measurements. Concerning the second aim, it is noted that the LNG carriers are about 300 m long, 50 m wide and the bridge is about 45 m above the sea level (Fig. 3a). Together with the current, wind forces are a main factor for these large ships for manoeuvring in the channel. The longitudinal wind component influences the speed of the ship, which must be 3 m/s or less to reduce the risk of damage to the LNG tanks in case of a grounding. The cross-wind component not only causes a lateral force, but also a turning moment, which affect the width required for the manoeuvring. Gradients in wind speed or direction over the length of the ship also cause a turning moment, which directly affects manoeuvring. To ensure that the results of manoeuvring simulations are representative for the day-to-day practice, it is essential that realistic and reasonably accurate mean wind-velocity fields are inserted into the simulator database. The present CFD study focuses on high wind speed conditions, for which the atmospheric boundary layer exhibits neutral stratification. The reason is that high wind speeds are most relevant for manoeuvring, due to the larger forces at higher wind speeds. Note that a reference wind speed U_{10} at 10 m height of 10 m/s is imposed as limiting condition for entering the channel by local regulations.

The distance between the entrance of the Ria and the LNG terminal is about 10 km. In aerodynamic studies, typically an upstream fetch of 5–10 km needs to be taken into account, because this is the distance over which the vertical atmospheric boundary layer (ABL) profiles of mean velocity and turbulence properties develop due to their interaction with the aerodynamic roughness length of the terrain (Wieringa, 1992). The study area is therefore larger than the extent of the Ria and is illustrated by the yellow rectangle in Fig. 4. The landscape topography in this area is described by Geographic Information System (GIS) data (Cartographia-Fotografia Aérea – S.A. Desenvolvemento Comarcal de Galiza) with a horizontal resolution of 10 m.

4. Field measurements

Field measurements of wind speed with two-dimensional ultrasonic anemometers have been made at five different positions A–E (Fig. 5a) for a period of four weeks. The UTM coordinates of the five positions are given in Table 1. Position A is the reference position, located on top of a crane at the Port Exterior, at a height of about 65 m above mean sea level (MSL) (Fig. 5b). The four other positions are different locations along the channel, at a height of about 10 m above the local terrain surface. Selecting good measurement positions was a difficult task. The criteria for selection were: (1) representativeness for wind conditions in the Ria; (2) avoiding local disturbance effects by small-scale terrain features that are not included in detail in the numerical model, such as individual buildings and trees; and (3) safety and theft protection of the equipment. Position A provides a good reference measurement position, because it is not significantly influenced by the surrounding terrain for most wind directions (Fig. 5b). Position B is situated at Cabo Prioriño, at a height of about 50 m above MSL, and is also a suitable measurement location (Fig. 5c). Position C is at the top of the beacon tower at Punta de San Martin, at a height of 2.1 m above the tower, and about 14 m above MSL (Fig. 5d). For this position, the presence of the beacon tower might have some influence on the measurements. Position D is at Castillo de La Palma, at a height of about 6.7 m above the surrounding balustrade, and about 12.7 m

Fig. 3. (a) Perspective view of Ria de Ferrol with LNG carrier assisted by tug boats (© Pedrotop); (b) perspective view with cruise ship (CC-BY 3.0, datuopinion.com 2011). View positions and directions are given in plan view subfigures in top right corners.

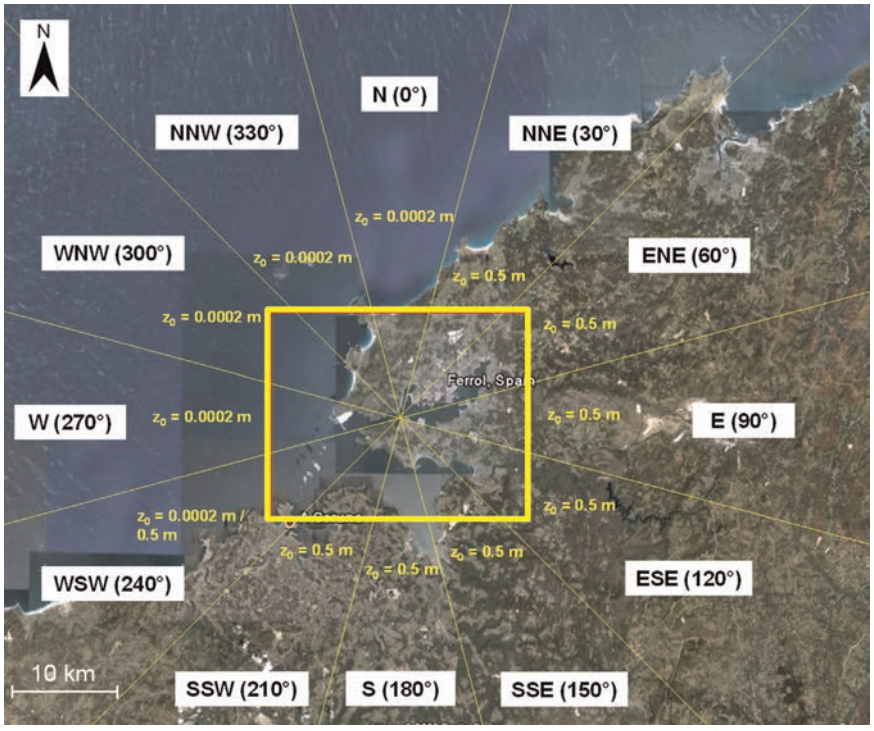

Fig. 4. Indication of the study area (yellow rectangle) and aerodynamic roughness lengths z_0 for the terrain surrounding the study area.

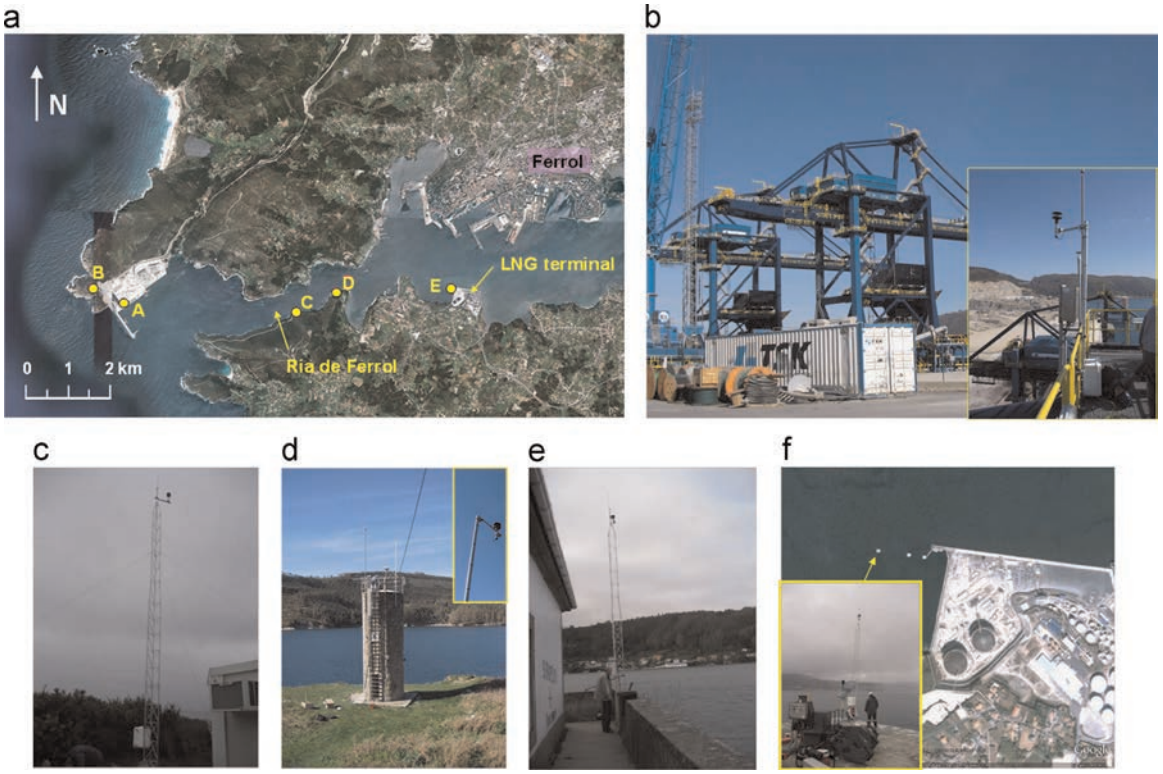

Fig. 5. (a) Indication of the five measurement positions A–E; (b) measurement position A on top of the crane at Port Exterior; (c) measurement position B at Cabo Prioriño; (d) measurement position C at the top of the beacon tower at Punta de San Martin; (e) measurement position D on balustrade of Castillo de La Palma; (f) measurement position E at outer northwest mooring dolphin of the terminal.

above MSL (Fig. 5e). For this position, a nearby building strongly influences the measurements, except for wind directions NW en SE. Only data from these wind directions will therefore be used for validation at this point. Finally, position E is placed at the outer northwest mooring dolphin of the terminal, at a height of about 11.7 m above MSL (Fig. 5f). This is a relatively unobstructed measurement position.

The gathered field measurements were 1-min data, which were converted (averaged) into 10-min data to more strongly position them in the spectral gap of the wind speed power spectrum (Van

Table 1
UTM coordinates of the five measurement positions.

Measurement position	Easting (m)	Northing (m)
A	554,079.02	4,812,301.73
B	553,552.59	4,812,881.73
C	558,020.02	4,812,351.09
D	558,911.69	4,812,765.31
E	561,381.98	4,812,773.79

der Hoven, 1957). The comparison between CFD results and experimental data was only made for those wind directions for which sufficient data satisfying two criteria were available. The first criterion was that the reference wind speed at point A has to be higher than 7 m/s. This is important to exclude thermal effects from the comparison. As mentioned before, the CFD simulations are performed for neutral atmospheric conditions, and thermal effects are ignored. Note that the manoeuvring simulations that will be based on the wind-velocity patterns – but that are not reported in this paper – are typically carried out for a reference wind speed $U_{10}=10$ m/s. The second criterion concerned wind direction selection. Around every of the 12 wind directions for which CFD simulations were made (0° - 30° - … - 330°), a relatively narrow 10° wind direction sector was defined. All experimental 10- min data values that had 10- min wind directions at point A within this sector, were averaged and standard deviations were obtained. This was only performed for those wind direction sectors with more than twenty 10- min data points. These averages will be compared with the corresponding CFD results in Section 6. Note that because of the above-mentioned two criteria, data for wind directions 90° and 120° were not available for comparison.

5. CFD simulations: computational settings and parameters

5.1. Computational geometry, domain and grid

The computational geometry is based on the GIS data with a horizontal resolution of 10 m. Only the data in the yellow rectangle in Fig. 4 are used, which bounds the horizontal area of the computational domain of 25×20.5 km^2. The height of the domain is 1 km. As mentioned earlier, the choice of the horizontal extent of the domain is based on the fact that a distance of about 5–10 km from the region of interest, being the entrance channel, is sufficient to numerically model the development of the approaching ABL due to the aerodynamic roughness length of the terrain. The GIS data are implemented as points, and surfaces are fit through these data points. Next, the surfaces are discretised with quadrilateral and triangular cells that provide the basis for the generation of 3D prismatic cells for application of the control volume method.

The computational grid (Figs. 6 and 7) is generated using the surface grid extrusion technique presented by van Hooff and Blocken (2010a). This technique allows a large degree of control over the size and shape of the computational cells. This grid technique only uses hexahedral and prismatic cells, and no tetrahedral and pyramid cells. In this case, all cell faces are either vertical, or parallel to the underlying terrain surface. This reduces the numerical discretisation error and allows the use of second-order discretisation schemes without compromising convergence. This technique has been successfully applied in other CFD studies to model complex urban areas (van Hooff and Blocken, 2010a, 2010b; Blocken et al., 2012; Montazeri et al., 2013; Toparlar et al., 2015; Gromke et al., 2015) and building geometries and building component details (van Hooff et al., 2011a, 2011b). For the present

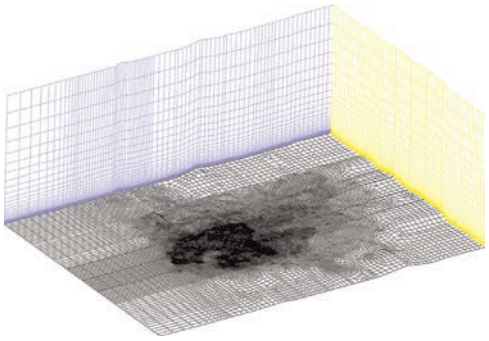

Fig. 6. Computational grid on the bottom surface and north and east vertical side surfaces of the domain. Total number of cells is 3,984,984.

simulation, the grid resolution in the vertical direction is 2.5 m for the first 10 m, and increases gradually with height above 10 m. The resulting grid contains 3,984,984 control volumes and is based on a grid-sensitivity analysis focused on mean wind speed in the entrance channel.

5.2. Boundary conditions and solver settings

A distinction is made between two types of roughness (Blocken et al., 2007a; Blocken, 2015): (1) the roughness of the terrain that is included in the computational domain and (2) the roughness of the terrain that is not included in the computational domain. The knowledge of the roughness of the terrain that is situated outside the computational domain is important because it determines the shape of the inlet profiles of mean wind speed and turbulence properties. These profiles are generally expressed as a function of the aerodynamic roughness length z_0 (Wieringa, 1992). This parameter can be determined based on a roughness estimation of the terrain that extends from the inlet of the computational domain up to about 5–10 km upstream of this inlet. This is done using the roughness classification of Davenport, updated by Wieringa (1992). Fig. 4 graphically represents the 12 wind direction sectors surrounding the computational domain and their z_0 values.

On the other hand, the roughness of the terrain inside the computational domain is important because it determines to a large extent the local flow conditions and the development of internal boundary layers in the domain. For CFD codes that use wall functions with a roughness modification based on the equivalent sand-grain roughness height k_S and the roughness constant C_S, such as the code ANSYS/Fluent 6.3 used in this study, three steps are required:

(1) subdivision of the terrain into patches with similar roughness (see Fig. 8);
(2) estimation of the local z_0 using the roughness classification (Wieringa, 1992); and
(3) conversion of z_0 into the corresponding wall function parameters k_S and C_S (Blocken et al., 2007a). These parameters can be calculated from z_0 using the appropriate conversion equation, which, for Fluent 6.3, was derived by (Blocken et al., 2007a):

$$k_{S,ABL} = \frac{9.793\ z_0}{C_s} \tag{1}$$

Fig. 8 also lists the resulting roughness categories and the roughness parameters. The importance of correct ground roughness specification for the accuracy of CFD simulation results in general was mentioned and/or demonstrated in earlier research (e.g. Richards and Hoxey (1993), Blocken et al. (2007a, 2007b), Hargreaves and

Wright (2007), Franke et al. (2007), Gorlé et al. (2009), Yang et al. (2009), Richards and Norris (2011), Parente et al. (2011)). The importance of surface roughness for wind flow over complex terrain in particular was also stressed by several previous authors (Lun et al. (2003), Prospathopoulos and Voutsinas (2006), Cao and Tamura (2006, 2007), Tamura et al. (2007), Wakes et al. (2010), Cao et al. (2012)). This was an extra reason to dedicate special attention to surface roughness specification in the present study.

Based on the first type of roughness (z_0 from Fig. 4), at the inlet of the domain, the inlet profiles of mean wind speed U, turbulent kinetic energy k and turbulence dissipation rate ε are imposed, using the equations by Richards and Hoxey (1993):

$$U(z) = \frac{u^*_{ABL}}{\kappa} \ln\left(\frac{z+z_0}{z_0}\right) \quad (2)$$

$$k(z) = u^{*2}_{ABL} \frac{}{\sqrt{C_\mu}} \quad (3)$$

$$\varepsilon(z) = \frac{u^{*3}_{ABL}}{\kappa(z+z_0)} \quad (4)$$

where u^*_{ABL} is the ABL friction velocity, κ the von Karman constant (0.42) and C_μ a constant equal to 0.09.

Based on the second type of roughness (z_0 from Fig. 8), for the ground surface, the standard wall functions by Launder and Spalding (1974) with roughness modification by Cebeci and Bradshaw (1977) and the appropriate parameters k_S and C_S are applied.

The sides and top of the domain are modelled as a slip walls (zero normal velocity and zero normal gradients of all variables). At the outlet, zero static pressure is set.

The 3D steady Reynolds-Averaged Navier–Stokes (RANS) equations are solved with the commercial CFD code ANSYS/Fluent 6.3 (Fluent Inc., 2006) using the control volume method. The realisable k–ε model (Shih et al., 1995) is used to provide closure. Second-order discretisation schemes are used for both the convective and viscous terms of the governing equations. The SIMPLE algorithm is used for pressure-velocity coupling and standard pressure interpolation is used. Calculations are performed for 12 wind directions: 0° - 30° - … - 330°. Convergence is assumed to be

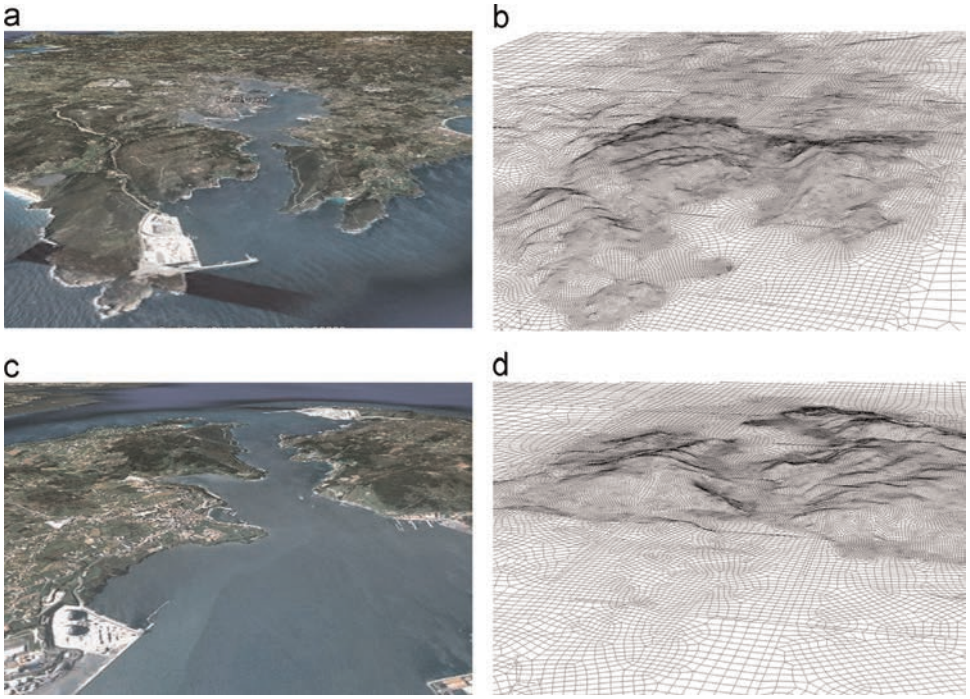

Fig. 7. (a, b) Perspective view from west of topography and computational grid on terrain surface; (c, d) Perspective view from east of topography and computational grid on terrain surface. Total number of cells is 3,984,984.

Type	Nr.	z_0 (m)	k_S (m)	C_S
Sea/estuary	I	0.0002 m	0.0039	0.5
Concrete/bare land	II	0.005 m	0.10	0.5
Grass land	III	0.03 m	0.59	0.5
Spread-out built environment	VI	0.5 m	1.25	3.92
Clumps of forest	VII	1 m	1.25	7.83
Ferrol centre	VII	1 m	1.25	7.83

Fig. 8. Subdivision of local terrain into patches based on roughness classification and corresponding roughness categories and parameters z_0, k_S and C_S.

obtained when all the scaled residuals (Fluent Inc., 2006) have levelled off.

6. CFD simulations: results

6.1. Comparison with on-site measurements

The values that are compared are the wind speed ratio and the wind direction. Two sets of wind speed ratios are distinguished:

(1) The wind speed ratios K at the measurement positions, which are related to the crane position A. This means that K is the wind speed at a measurement position divided by the wind speed at position A.
(2) The wind speed ratios K_{10} at a height of 10 m above MSL, which are related to the reference wind speed over open sea at 10 m above MSL. This means that K_{10} is the local horizontal wind speed at 10 m divided by the horizontal reference wind speed over open sea at the same height. Note that the wind speed over open sea corresponds to the logarithmic law for the neutral atmospheric boundary layer with an aerodynamic roughness length $z_0 = 0.0002$ m.

The numerically simulated values at the measurement positions have been obtained from the CFD results by 3D interpolation from the neighbouring cell centre values. Figs. 9–12 illustrate the colour contours of simulated wind speed ratio K_{10} at 10 m height above MSL, together with the simulated and measured wind speed ratio vectors K at the five measurement positions, for reference (i.e. inlet) wind directions 60°, 210°, 240° and 300°. The tables in the top left corner of the figures provide the mean and standard deviations of the measured values of K and the wind direction PHI, as well as the simulated (numerical) values. For all positions except position D, a good to very good agreement is obtained. The numerically simulated wind speed ratios and wind directions are generally situated within the standard deviations of the measurements. As mentioned earlier, at position D, the presence of a nearby building affects the measurement accuracy.

Fig. 13a compares the simulated and measured wind speed ratio K for all five measurement positions and for ten different wind directions, illustrating the good agreement for each of these directions. The numerical values are generally within 10–20% of the corresponding measurements. Fig. 13b provides the same information for simulated and measured wind directions. The numerical values show deviations from the measurement values that are generally less than 30°.

6.2. Simulated wind-flow patterns

Based on the successful validation study, the wind-flow patterns for each of the 12 wind directions can be analysed. Fig. 14 shows contours of the wind speed ratio K_{10} in a horizontal plane at 10 m height above MSL, for all 12 wind directions. The following observations are made:

- The figures show the spatial variation of wind speed in the Ria. The irregular hilly terrain yields large wind speed gradients.
- For wind directions 0°, 150°, 180° and 330°, the topography of the surrounding terrain provides the largest sheltering effects in the channel.
- For wind directions 60°, 90°, 240° and 270°, which are aligned with the channel, a funnelling effect occurs. For wind directions 60° and 90°, the wind speed ratio in the channel is between 0.9 and 1. For wind directions 240° and 270° however, the wind speed ratio in the channel is larger than 1. This increase is due to the upstream terrain roughness, which is less for the latter two

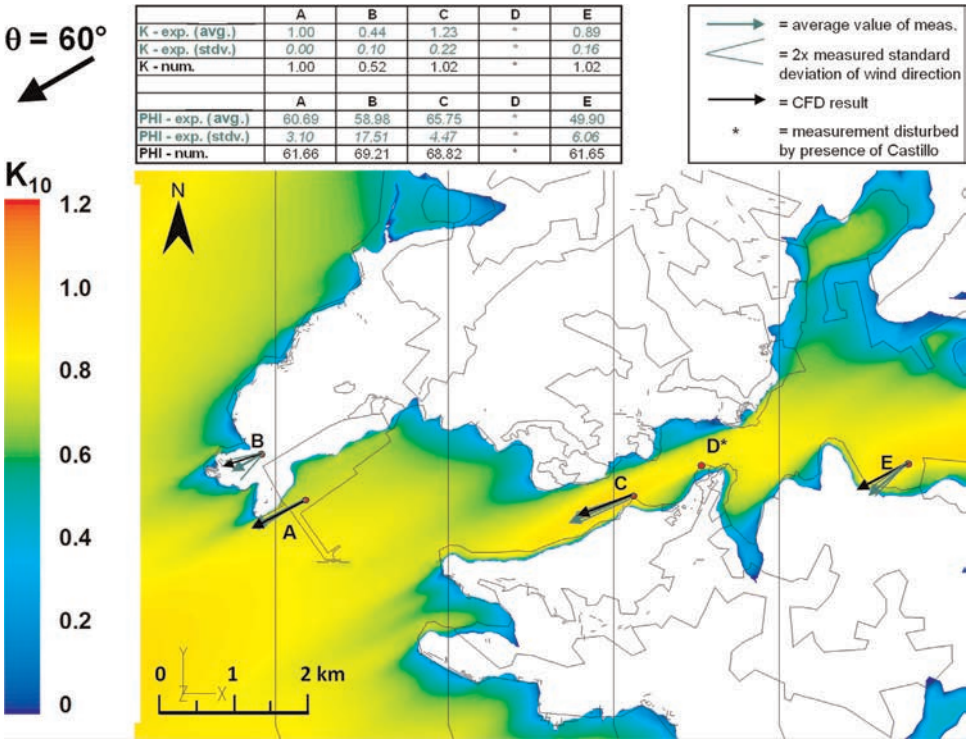

	A	B	C	D	E
K - exp. (avg.)	1.00	0.44	1.23	*	0.89
K - exp. (stdv.)	0.00	0.10	0.22	*	0.16
K - num.	1.00	0.52	1.02	*	1.02

	A	B	C	D	E
PHI - exp. (avg.)	60.69	58.98	65.75	*	49.90
PHI - exp. (stdv.)	3.10	17.51	4.47	*	6.06
PHI - num.	61.66	69.21	68.82	*	61.65

Fig. 9. Colour contours of simulated wind speed ratio K_{10} in a horizontal plane at 10 m height above mean sea level for reference wind direction $\theta = 60°$. Wind speed ratio vectors K at measurement positions: simulated (black) versus measured (green), with indication of standard deviation (green). Average values and standard deviations are given in the table in the upper left corner. Note: K_{10} and K are defined in a different way, related to different reference wind speed values. (For interpretation of the references to colour in this figure legend, the reader is referred to the web version of this article.)

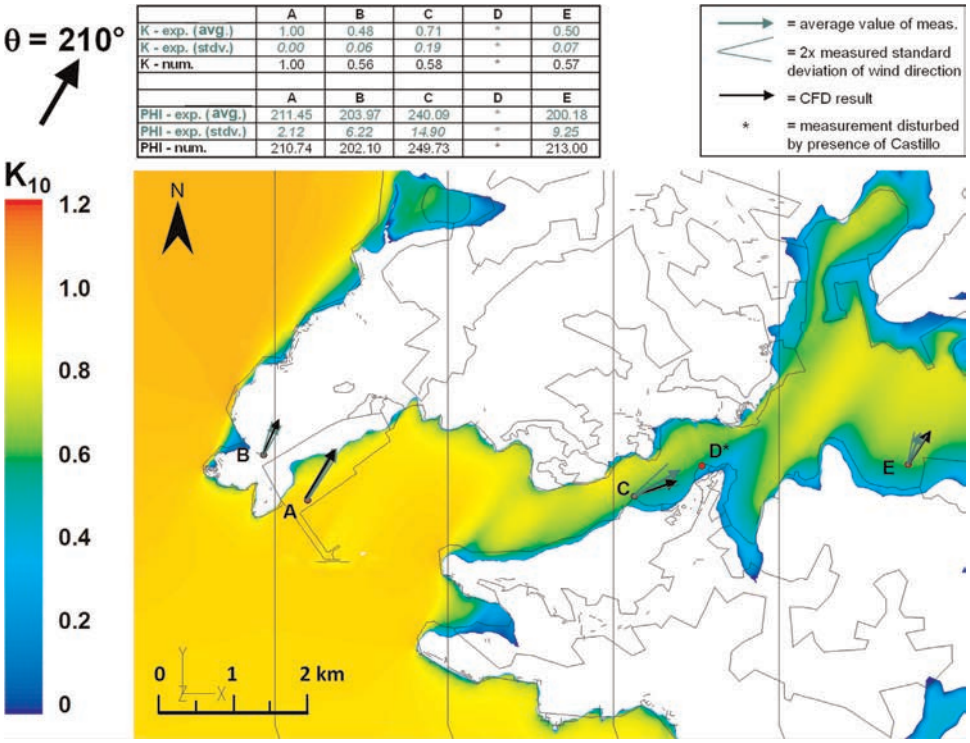

	A	B	C	D	E
K - exp. (avg.)	1.00	0.48	0.71	*	0.50
K - exp. (stdv.)	0.00	0.06	0.19	*	0.07
K - num.	1.00	0.56	0.58	*	0.57
	A	B	C	D	E
PHI - exp. (avg.)	211.45	203.97	240.09	*	200.18
PHI - exp. (stdv.)	2.12	6.22	14.90	*	9.25
PHI - num.	210.74	202.10	249.73	*	213.00

Fig. 10. Colour contours of simulated wind speed ratio K_{10} in a horizontal plane at 10 m height above mean sea level for reference wind direction θ=210°. Wind speed ratio vectors K at measurement positions: simulated (black) versus measured (green), with indication of standard deviation (green). Average values and standard deviations are given in the table in the upper left corner. Note: K_{10} and K are defined in a different way, related to different reference wind speed values. (For interpretation of the references to colour in this figure legend, the reader is referred to the web version of this article.)

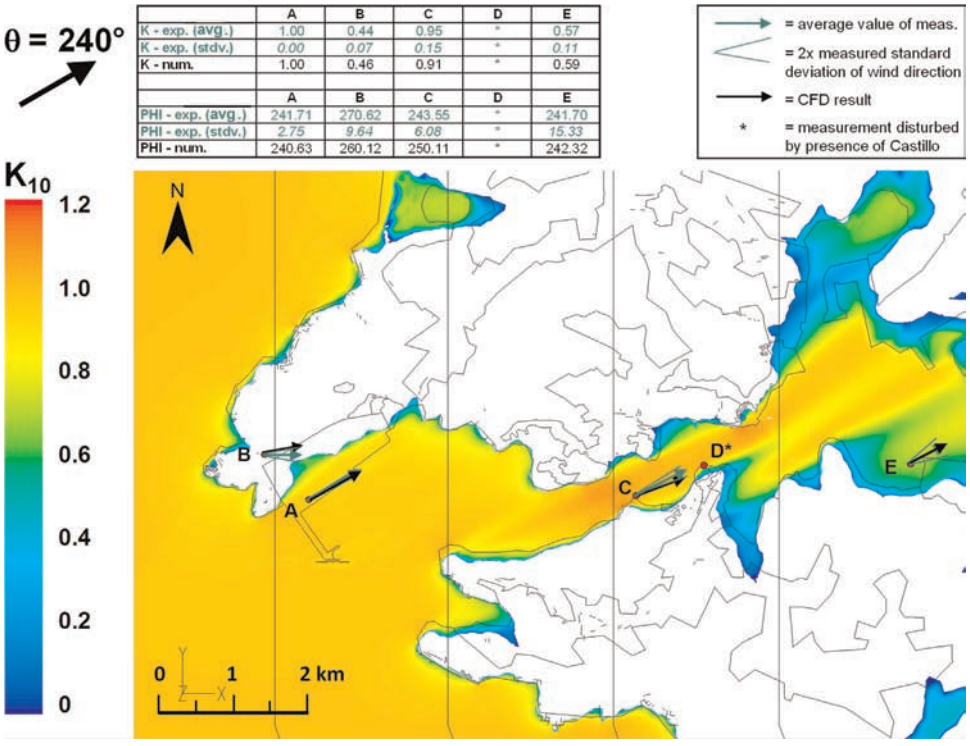

	A	B	C	D	E
K - exp. (avg.)	1.00	0.44	0.95	*	0.57
K - exp. (stdv.)	0.00	0.07	0.15	*	0.11
K - num.	1.00	0.46	0.91	*	0.59
	A	B	C	D	E
PHI - exp. (avg.)	241.71	270.62	243.55	*	241.70
PHI - exp. (stdv.)	2.75	9.64	6.08	*	15.33
PHI - num.	240.63	260.12	250.11	*	242.32

Fig. 11. Colour contours of simulated wind speed ratio K_{10} in a horizontal plane at 10 m height above mean sea level for reference wind direction θ=240°. Wind speed ratio vectors K at measurement positions: simulated (black) versus measured (green), with indication of standard deviation (green). Average values and standard deviations are given in the table in the upper left corner. Note: K_{10} and K are defined in a different way, related to different reference wind speed values. (For interpretation of the references to colour in this figure legend, the reader is referred to the web version of this article.)

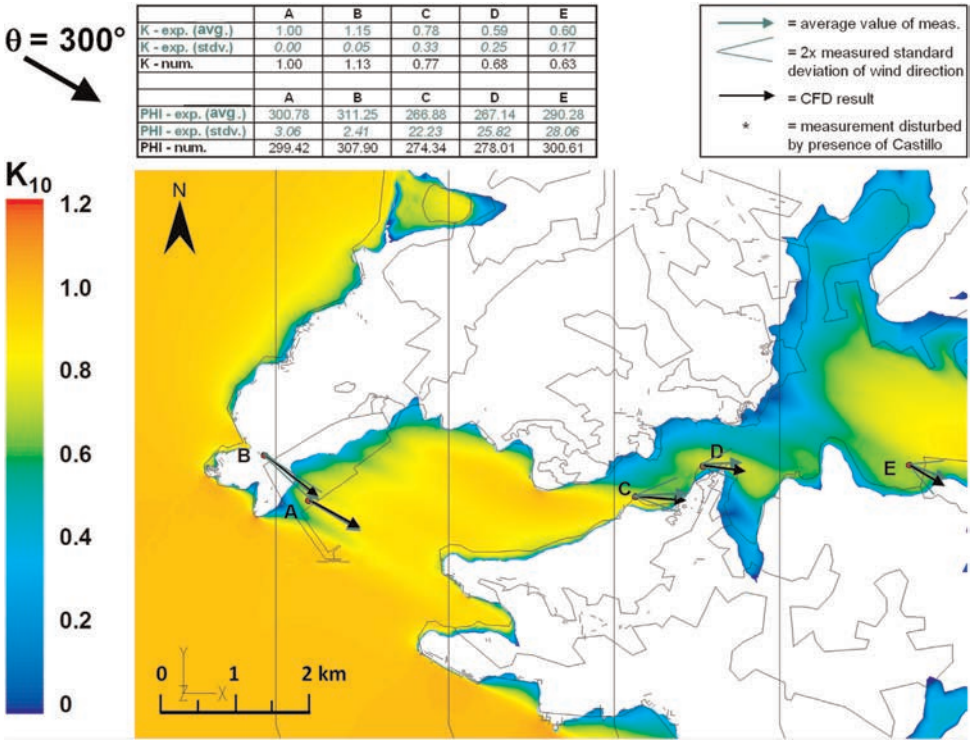

Fig. 12. Colour contours of simulated wind speed ratio K_{10} in a horizontal plane at 10 m height above mean sea level for reference wind direction $\theta = 300°$. Wind speed ratio vectors K at measurement positions: simulated (black) versus measured (green), with indication of standard deviation (green). Average values and standard deviations are given in the table in the upper left corner. Note: K_{10} and K are defined in a different way, related to different reference wind speed values. (For interpretation of the references to colour in this figure legend, the reader is referred to the web version of this article.)

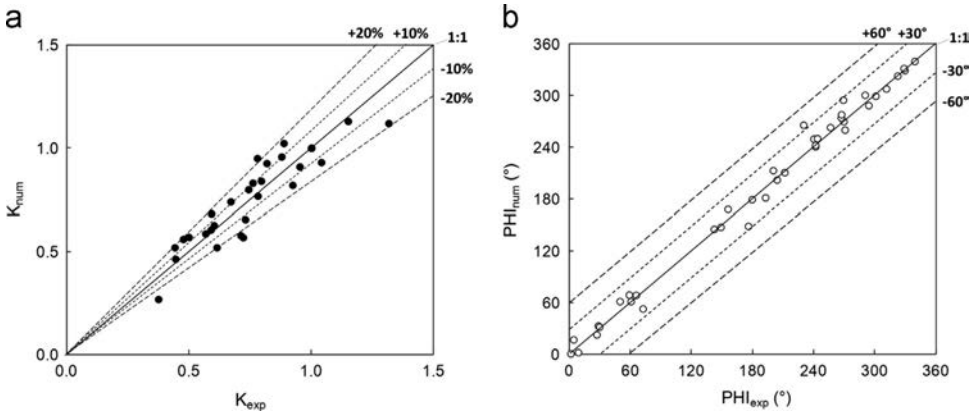

Fig. 13. (a) Comparison of numerically simulated and experimentally measured wind speed ratio K at the five measurement positions for ten different reference wind directions. (b) Same, for local wind direction PHI (° from north).

wind directions, where the wind approaches over sea and is amplified in the channel.
- For the other wind directions, strong gradients are present along the channel axis. This is of particular relevance for manoeuvring as on certain positions the stern and the bow of the ship will experience large differences in cross-wind forces.

7. Discussion

In this case study, 3D steady RANS with the realisable k–ε model is applied to simulate mean wind-velocity patterns in a narrow entrance channel. The simulation results are compared with on-site measurements at five positions.

7.1. Limitations and assumptions

The study is based on several assumptions:

- Only the overall topography was explicitly included in the model. Small-scale topographic features such as individual buildings and trees were not modelled explicitly, but only implicitly, by means of adjusted parameters k_S and C_S in the roughness modification of the wall functions.
- The aerodynamic roughness length z_0 of the sea surface depends on the wind speed through the interaction between wind and waves. In the present study, the value of z_0 was extracted from the Davenport–Wieringa roughness classification. No attempt was made to categorise the experimental data in wind speed classes and to perform numerical simulations

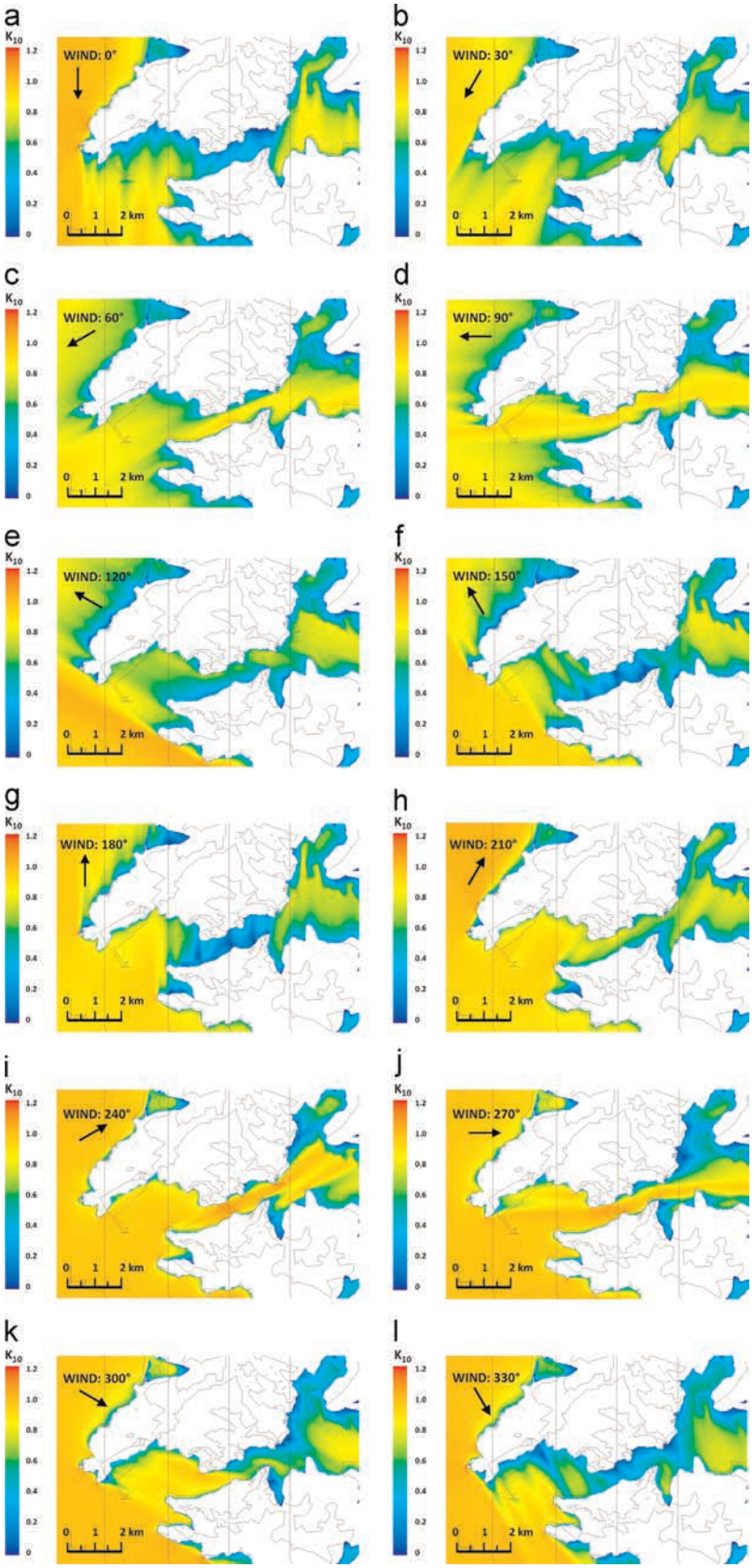

Fig. 14. Contours of numerically simulated wind speed ratio K_{10} in a horizontal plane at 10 m height above mean sea level, for reference wind directions 0°–330°.

with different z_0 values for the sea surface. Note however that the focus in this study was on high wind speed; the current limit mean wind speed at which ships are still allowed to enter the channel is 10 m/s. Also only experimental data with wind speed at position A larger than 7 m/s were retained for validation purposes.

- An additional simplification was the fact that the simulations were only performed for a neutrally-stratified atmospheric boundary layer flow. This is considered justified because the focus is on high wind speed.
- The CFD simulations were performed with the steady RANS approach. This was considered justified because the intention of the study was to determine the relationship between the 10- min mean wind speed and direction at every position in the Ria and the 10- min mean wind speed and direction over open sea. The intention was not to provide information on turbulence intensities or to perform long transient calculations to determine the local wind climate. If more detailed information on turbulence intensity or other transient characteristics are required, one would need to resort to the LES approach.
- In high wind speed flow, the turbulent stresses, which vary as the square of velocity, will largely exceed the Coriolis forces, therefore the latter are neglected.

In spite of these limitations, the numerical simulations in general showed a good to very good agreement with the experiments. An additional limitation of the study is that measurements were only made at 5 positions. While these positions were quite representative for the wind conditions in the channel, validation with more measurement points would have been beneficial.

Finally, it is mentioned that these results are currently being used for real-time manoeuvring simulations of LNG carriers (not reported in this paper). For this purpose, the results of the numerical wind calculations at 10 and 40 m above mean sea level were exported on a 9×4 km^2 regular grid covering the narrow entrance channel with a resolution of 25 m in both x and y direction, and were converted to wind forces on the ship using wind pressure coefficient databases for the ship geometry.

7.2. CFD simulations versus wind-tunnel modelling

Concerning the second aim of the study, i.e. to provide mean wind-velocity data for real-time manoeuvring simulations of LNG carriers, the combination of CFD simulations validated by field measurements at a few selected positions was considered the best option. Field measurements alone would have provide insufficient spatial data points. CFD was preferred over wind-tunnel modelling. The absolute minimum horizontal distance that should be modelled is that between the entrance of the Ria and the LNG terminal, which is about 10 km (Fig. 2). If the study of wind conditions would be performed in an Atmospheric Boundary Layer (ABL) wind tunnel, the reduced-scale model should therefore correspond to a full-scale situation of at least 10 km in diameter. Even for a large ABL wind tunnel with a test section of 3 m width, a scaling factor of at least 3500 would be required. For mean wind velocity at a height $H=10$ m above mean sea level in the Ria, the full-scale Reynolds number for a reference wind speed of $U_{10}=10$ m/s is $\mathrm{Re}=U_{10}\mathrm{H}/\nu=6.8\times10^6$, while the corresponding reduced-scale value would be $\mathrm{Re}\approx2000$, which is near the laminar regime. It is unlikely that accurate results can be obtained with such a strong reduction in Reynolds number.

8. Conclusions

Accurate and reliable Computational Fluid Dynamics (CFD) simulations of wind flow over natural complex terrain are important for a wide range of applications including dispersion of pollutants, wind energy resource assessment and ship manoeuvring in channels and near harbours. In the past 50 years, a very large number of CFD studies of wind flow over hills have been performed. However, a detailed review of the literature shows a lack of CFD studies including validation by field measurements for natural complex terrain beyond the case of isolated hills. Therefore, this paper presents a CFD study with field measurement validation for natural complex terrain that consists of an irregular succession of hills and valleys surrounding a narrow entrance channel, i.e. Ria de Ferrol in Galicia, Spain. The 400–500 m wide channel connects the LNG terminal of Reganosa in Mugardos with the sea. It is enclosed by irregular hilly terrain up to about 250 m above sea level, which was expected to yield complex wind-flow patterns.

The case study is performed using 3D steady RANS simulations with the realisable k–ε model to provide mean wind velocity in and around the narrow entrance channel. The study focused on high wind speed conditions, for which the atmospheric boundary layer exhibits neutral stratification. The aim of the study was twofold: (1) to evaluate the accuracy of 3D steady RANS with a revised k–ε model for calculating mean wind-velocity patterns over natural complex terrain; and (2) to provide mean wind velocity data that can be used as input for real-time manoeuvring simulations to evaluate accessing the LNG terminal with larger LNG carriers.

Concerning the first aim, particular attention is given to the generation of a high-quality computational grid, to surface roughness parameterisation and specification and to validation of the CFD simulations with field measurements. The comparison of the results of the CFD simulations with the measurements shows a good to very good agreement, with deviations that are generally within 10–20%. Both the numerical and the measured results illustrate the complexity of the mean wind-flow pattern and the funnelling effect by the topography on the wind for some specific wind directions. The study shows that for the present application, the 3D steady RANS approach with the realisable k–ε model can provide an accurate assessment of the complex mean wind-flow patterns and the funnelling effect by the topography on the wind.

Concerning the second aim, CFD was chosen because wind-tunnel modelling of these conditions was inhibited by the large geometrical dimensions of the channel and its surrounding topography, which would require too large scaling factors in a typical-size ABL wind tunnel and too strong violation of similarity requirements. the study has shown that for wind directions 60° and 90°, the funnelling effect leads to an increase of wind speed in the channel compared to the wind speed over open sea. For other wind directions, the topography leads to a reduction of the wind speed in the channel, but also to strong wind speed gradients along the channel axis, which are important for ship manoeuvring. The results of this study are currently being used for real-time manoeuvring simulations of LNG carriers in Ria de Ferrol.

Acknowledgements

Reganosa is acknowledged for their kind permission to use the CFD results and measured wind data of the studies for the access of large LNG carriers for this publication. The numerical simulations reported in this paper were supported by the laboratory of the Unit Building Physics and Services (BPS) of Eindhoven University of Technology.

References

Apsley, D.D., 1995. Numerical Modelling of Neutral and Stably Stratified Flow and Dispersion in Complex Terrain (Ph.D. thesis). University of Surrey, UK.
Apsley, D.D., Castro, P.I., 1997a. Numerical modelling of flow and dispersion around Cinder Cone Butte. Atmos. Environ. 31 (7), 1059–1071.

Apsley, D.D., Castro, I.P., 1997b. Flow and dispersion over hills: comparison between numerical predictions and experimental data. J. Wind Eng. Ind. Aerodyn. 67–68, 375–386.
Apsley, D.D., Castro, I.P., 1997c. A limited-length-scale k-ε model for the neutral and stably-stratified atmospheric boundary layer. Bound.-Layer Meteorol. 83, 75–98.
Baker, C.J., 2007. Wind engineering – Past, present and future. J. Wind Eng. Ind. Aerodyn. 95 (9–11), 843–870.
Balogh, M., Parente, A., Benocci, C., 2012. RANS simulation of ABL flow over complex terrain applying an enhanced k-ε model and wall function formulation: Implementation and comparison for Fluent and OpenFOAM. J. Wind Eng. Ind. Aerodyn. 104–1069, 360–368.
Bechmann, A., Berg, J., Courtney, M., Jorgensen, H., Mann, J., Sorensen, N., 2009. The Bolund experiment: overview and background. Riso DTU Report Riso-R1658 (EN), (50 pp.).
Bechmann, A., Sorensen, N.N., 2010. Hybrid RANS/LES method for wind flow over complex terrain. Wind Energy 13, 36–50.
Bechmann, A., Sorensen, N.N., Berg, J., Mann, J., Réthoré, P.E., 2011. The Bolund experiment, part II: blind comparison of microscale flow models. Bound.-Layer Meteorol. 141, 245–271.
Berg, J., Mann, J., Bechmann, A., Courtney, M., Jorgensen, H., 2011. The Bolund experiment, part I: flow over a steep, three-dimensional hill. Bound.-Layer Meteorol. 141 (2), 219–243.
Bitsuamlak, G., Stathopoulos, T., Bédard, C., 2004. Numerical evaluation of wind flow over complex terrain: review. J. Aerosp. Eng. 17 (4), 135–145.
Bitsuamlak, G., Stathopoulos, T., Bédard, C., 2006. Effect of upstream hills on design wind load: a computational approach. Wind Struct. 9 (1), 37–58.
Blocken, B., Carmeliet, J., 2004. A review of wind-driven rain research in building science. J. Wind Eng. Ind. Aerodyn. 92 (13), 1079–1130.
Blocken, B., Stathopoulos, T., Carmeliet, J., 2007a. CFD simulation of the atmospheric boundary layer: wall function problems. Atmos. Environ. 41 (2), 238–252.
Blocken, B., Carmeliet, J., Stathopoulos, T., 2007b. CFD evaluation of the wind speed conditions in passages between buildings – effect of wall-function roughness modifications on the atmospheric boundary layer flow. J. Wind Eng. Ind. Aerodyn. 95 (9–11), 941–962.
Blocken, B., Carmeliet, J., 2010. Overview of three state-of-the-art wind-driven rain assessment models and comparison based on model theory. Build. Environ. 45 (3), 691–703.
Blocken, B., Stathopoulos, T., Carmeliet, J., Hensen, J.L.M., 2011. Application of CFD in building performance simulation for the outdoor environment: an overview. J. Build. Perform. Simul. 4 (2), 157–184.
Blocken, B., Janssen, W.D., van Hooff, T., 2012. CFD simulation for pedestrian wind comfort and wind safety in urban areas: general decision framework and case study for the Eindhoven University campus. Environ. Model. Softw. 30, 15–34.
Blocken, B., Gualtieri, C., 2012. Ten iterative steps for model development and evaluation applied to computational fluid dynamics for environmental fluid mechanics. Environ. Model. Softw. 33, 1–22.
Blocken, B., Tominaga, Y., Stathopoulos, T., 2013. CFD simulation of micro-scale pollutant dispersion in the built environment. Build. Environ. 64, 225–230.
Blocken, B., Stathopoulos, T., 2013. Editorial to virtual special issue: CFD simulation of pedestrian-level wind conditions around buildings: past achievements and prospects. J. Wind Eng. Ind. Aerodyn. 121, 138–145.
Blocken, B., 2014. 50 years of computational wind engineering: past, present and future. J. Wind Eng. Ind. Aerodyn. 129, 69–102.
Blocken, B., 2015. Computational fluid dynamics for urban physics: importance, scales, possibilities, limitations and ten tips and tricks towards accurate and reliable simulations. Build. Environ. 91, 219–245.
Britter, R., Schatzmann, M. (Eds.), 2007. Model Evaluation Guidance and Protocol Document COST Action 732. COST Office Brussels, Belgium, ISBN 3-00-018312-4.
Canepa, E., 2004. An overview about the study of downwash effects on dispersion of airborne pollutants. Environ. Model. Softw. 19 (12), 1077–1087.
Cao, S., Tamura, T., 2006. Experimental study on roughness effects on turbulent boundary layer flow over a two-dimensional steep hill. J. Wind Eng. Ind. Aerodyn. 94, 1–19.
Cao, S., Tamura, T., 2007. Effects of roughness blocks on atmospheric boundary layer flow over a two-dimensional low hill with/without sudden roughness change. J. Wind Eng. Ind. Aerodyn. 95, 679–695.
Cao, S., Wang, T., Ge, Y., Tamura, Y., 2012. Numerical study on turbulent boundary layers over two-dimensional hills – effects of surface roughness and slope. J. Wind Eng. Ind. Aerodyn. 104–106, 342–349.
Casey, M., Wintergerste, T., 2000. Best Practice Guidelines, ERCOFTAC Special Interest Group on Quality and Trust in Industrial CFD. ERCOFTAC, Brussels.
Castro, F.A., JMLM, Palma, Silva Lopes, A., 2003. Simulation of the Askervein flow. Part 1: Reynolds Averaged Navier–Stokes equations (k–ε) turbulence model. Bound.-Layer Meteorol. 107, 501–530.
Cebeci, T., Bradshaw, P., 1977. Momentum Transfer in Boundary Layers. Hemisphere Publishing Corporation, New York.
Celik, I., Klein, M., Janicka, J., 2009. Assessment measures for engineering LES applications. J. Fluids Eng. 131, 10.
Chaudhari, A., 2014. Large-eddy simulation of wind flows over complex terrains for wind energy applications (Ph.D. thesis). Acta Universitatis Lappeenrantaensis 598, Lappeenranta University of Technology, Finland.
Conan, B., van Beeck, J., Aubrun, S., 2012. Sand erosion technique applied to wind resource assessment. J. Wind Eng. Ind. Aerodyn. 104–106, 322–329.
Dawson, P., Stock, D.E., Lamb, B., 1991. The numerical simulation of airflow and dispersion in three-dimensional atmospheric recirculation zones. J. Appl. Meteorol. 30, 1005–1024.
Detering, H.W., Etling, D., 1985. Application of the E–ε turbulence model to the atmospheric boundary layer. Bound.-Layer Meteorol. 33, 113–133.
Diebold, M., Higgins, C., Fang, J., Bechmann, A., Parlange, M., 2013. Flow over hills: a large-eddy simulation of the bolund case. Bound.-Layer Meteorol. 148 (1), 177–194.
Di Sabatino, S., Buccolieri, R., Salizzoni, P., 2013. Recent advancements in numerical modelling of flow and dispersion in urban areas: a short review. Int. J. Environ. Pollut. 52 (3–4), 172–191.
Fluent Inc, 2006. Fluent 6.3 User's Guide. Fluent Inc., Lebanon.
Franke, J., Hirsch, C., Jensen, A.G., Krüs, H.W., Schatzmann, M., Westbury, P.S., Miles, S.D., Wisse, J.A., Wright, N.G., 2004. Recommendations on the use of CFD in wind engineering. In: van Beeck, J.P.A.J. (Ed.), Proceedings of International Conference on Urban Wind Engineering and Building Aerodynamics, COST Action C14, Impact of Wind and Storm on City Life Built Environment, 5–7 May 2004. von Karman Institute, Sint-Genesius-Rode, Belgium.
Franke, J., Hellsten, A., Schlünzen, H., Carissimo, B., 2007. Best practice guideline for the CFD simulation of flows in the urban environment. COST 732: Quality Assurance and Improvement of Microscale Meteorological Models.
Franke, J., Hellsten, A., Schlünzen, H., Carissimo, B., 2011. The COST 732 best practice guideline for CFD simulation of flows in the urban environment – a summary. Int. J. Environ. Pollut. 44 (1–4), 419–427.
Gorlé, C., van Beeck, J., Rambaud, P., Van Tendeloo, G., 2009. CFD modelling of small particle dispersion: the influence of the turbulence kinetic energy in the atmospheric boundary layer. Atmos. Environ. 43 (3), 673–681.
Gousseau, P., Blocken, B., van Heijst, G.J.F., 2013. Quality assessment of Large-Eddy Simulation of wind flow around a high-rise building: validation and solution verification. Comput. Fluids 79, 120–133.
Gromke, C.B., Blocken, B., Janssen, W.D., Merema, B., van Hooff, T., Timmermans, H.J. P., 2015. CFD analysis of transpirational cooling by vegetation: case study for specific meteorological conditions during a heat wave in Arnhem, Netherlands. Build. Environ. 83, 11–26.
Hanna, S.R., 1989. Plume dispersion and concentration fluctuations in the atmosphere. Encyclopedia of environmental control technology. Air Pollution Control, 2. Gulf Publishing Company, Houston, TX, pp. 547–582.
Hargreaves, D.M., Wright, N.G., 2007. On the use of the k–ε model in commercial CFD software to model the neutral atmospheric boundary layer. J. Wind Eng. Ind. Aerodyn. 95 (5), 355–369.
Hewer, F.E., 1998. Non-linear numerical model predictions of flow over an isolated hill of moderate slope. Bound.-Layer Meteorol. 87, 381–408.
Hino, M., 1968. Computer experiment on smoke diffusion over a complicated topography. Atmos. Environ. 2, 541–558.
Jackson, P.S., Hunt, J.C.R., 1975. Turbulent wind flow over a low hill. Q. J. R. Meteorol. Soc. 101, 929–955.
Jiru, T.E., Bitsuamlak, G.T., 2010. Application of CFD in modelling wind-induced natural ventilation of buildings – a review. Int. J. Vent. 9 (2), 131–147.
Kim, H.G., Patel, V.C., Lee, C.M., 2000. Numerical simulation of wind flow over hilly terrain. J. Wind Eng. Ind. Aerodyn. 87, 45–60.
Klein, M., 2005. An attempt to assess the quality of large eddy simulations in the context of implicit filtering. Flow Turbul. Combust. 75, 131–147.
Launder, B.E., Spalding, D.B., 1974. The numerical computation of turbulent flows. Comput. Methods Appl. Mech. Eng. 3, 269–289.
Lavery, T.F., Bass, A., Strimaitis, D.G., Venkatram, A., Green, B.R., Drivas, P.J., 1982. EPA Complex Terrain Model Development: First Milestone Report (US EPA Report EPA-600/3-82-036).
Lee, J.T., Meroney, R.N., 1988, Numerical modeling of dense gas cloud dispersion over irregular terrain. In: Proceedings of 8th Symposium on Turbulence and Diffusion, AMS, 25–29 April 1988. Sand Diego, CA, p. 10.
Lun, Y.F., Mochida, A., Murakami, S., Yoshino, H., Shirasawa, T., 2003. Numerical simulation of flow over topographic features by revised k–ε models. J. Wind Eng. Ind. Aerodyn. 91, 231–245.
Mason, P.J., Sykes, R.I., 1979. Flow over an isolated hill of moderate slope. Q. J. R. Meteorol. Soc. 105, 383–395.
Meroney, R.N., 2004. Wind tunnel and numerical simulation of pollution dispersion: a hybrid approach. Working paper, Croucher Advanced Study Insitute on Wind Tunnel Modeling, Hong Kong University of Science and Technology, 6–10 December 2004, 60 pp.
Meroney, R.N., Derickson, R., 2014. Virtual reality in wind engineering: the windy world within the computer. J. Wind Eng. 11 (2), 11–26.
Meroney, R.N., 1990. Fluid dynamics of flow over hills and mountains: insights obtained through physical modeling, chapter 7 of AMS monograph on current directions in atmospheric processes over compex terrain. AMS Monogr. 23 (45), 145–172.
Meroney, R.N., 2012. CFD modeling of dense gas cloud dispersion over irregular terrain. J. Wind Eng. Ind. Aerodyn. 104–106, 500–508.
Metha, D., van Zuijlen, A.H., Koren, B., Holierhoek, J.G., Bijl, H., 2014. Large eddy simulation of wind farm aerodynamics: a review. J. Wind Eng. Ind. Aerodyn. 133, 1–17.
Mochida, A., Lun, I.Y.F., 2008. Prediction of wind environment and thermal comfort at pedestrian level in urban area. J. Wind Eng. Ind. Aerodyn. 96 (10–11), 1498–1527.
Mochida, A., Iizuka, S., Tominaga, Y., Lun, I.Y.F., 2011. Up-scaling CWE models to include mesoscale meteorological influences. J. Wind. Eng. Ind.Aerodyn. 99, 187–198.

Montazeri, H., Blocken, B., Janssen, W.D., van Hooff, T., 2013. CFD evaluation of new second-skin facade concept for wind comfort on building balconies: case-study for the Park Tower in Antwerp. Build. Environ. 68, 179–192.
Moonen, P., Defraeye, T., Dorer, V., Blocken, B., Carmeliet, J., 2012. Urban Physics: Effect of the micro-climate on comfort, health and energy demand. Front. Archit. Res. 1 (3), 197–228.
Moreira, G.A.A., dos Santos, A.A.C., do Nascimento, C.A.M., Valle, R.M., 2012. Numerical study of the neutral atmospheric boundary layer over complex terrain. Bound.-Layer Meteorol. 143, 393–407.
Murakami, S., 1993. Comparison of various turbulence models applied to a bluff body. J. Wind Eng. Ind. Aerodyn. 46–47, 21–36.
Murakami, S., 1997. Current status and future trends in computational wind engineering. J. Wind Eng. Ind. Aerodyn. 67–68, 3–34.
Murakami, S., 1998. Overview of turbulence models applied in CWE-1997. J. Wind Eng. Ind. Aerodyn. 74–76, 1–24.
Murakami, S., Ooka, R., Mochida, A., Yoshida, S., Kim, S., 1999. CFD analysis of wind climate from human scale to urban scale. J. Wind Eng. Ind. Aerodyn. 81, 57–81.
Norton, T., Sun, D.W., Grant, J., Fallon, R., Dodd, V., 2007. Applications of computational fluid dynamics (CFD) in the modelling and design of ventilation systems in the agricultural industry: a review. Bioresour. Technol. 98 (12), 2386–2414.
Ohba, R., Hara, T., Nakamura, S., Ohya, Y., Uchida, T., 2002. Gas diffusion over an isolated hill under neutral, stable and unstable conditions. Atmos. Environ. 36, 5697–5707.
Palma, J.M.L.M., Castro, F.A., Ribeiro, L.F., Rodrigues, A.H., Pinto, A.P., 2008. Linear and nonlinear models in wind resource assessment and wind turbine micro-siting in complex terrain. J. Wind Eng. Ind. Aerodyn. 96, 2308–2326.
Parente, A., Gorlé, C., van Beeck, J., Benocci, C., 2011. Improved k–ε model and wall function formulation for the RANS simulation of ABL flows. J. Wind Eng. Ind. Aerodyn. 99 (4), 267–278.
Porté-Agel, F., Wu, Y.T., Lu, H., Conzemius, R.J., 2011. Large-eddy simulation of atmospheric boundary layer flow through wind turbines and wind farms. J. Wind Eng. Ind. Aerodyn. 99 (4), 154–168.
Prospathopoulos, J., Voutsinas, S.G., 2006. Implementation issues in 3D wind flow predictions over complex terrain. J. Sol. Energy Eng. 128, 539–552.
Prospathopoulos, J.M., Politis, E.S., Chaviaropoulos, P.K., 2012. Application of a 3D RANS solver on the complex hill of Bolund and assessment of the wind flow predictions. J. Wind Eng. Ind. Aerodyn 107-108, 149–159.
Raithby, G.D., Stubley, G.D., Taylor, P.A., 1987. The Askervein hill project: a finite control volume prediction of three-dimensional flows over the hill. Bound.-Layer Meteorol. 39, 247–267.
Ramponi, R., Blocken, B., 2012a. CFD simulation of cross-ventilation for a generic isolated building: impact of computational parameters. Build. Environ. 53, 34–48.
Reichrath, S., Davies, T.W., 2002. Using CFD to model the internal climate of greenhouses: past, present and future. Agronomie 22, 3–19.
Richards, P.J., Hoxey, R.P., 1993. Appropriate boundary conditions for computational wind engineering models using the k–ε turbulence model. J. Wind Eng. Ind. Aerodyn. 46–47, 145–153.
Richards, P.J., Norris, S.E., 2011. Appropriate boundary conditions for computational wind engineering models revisited. J. Wind Eng. Ind. Aerodyn. 99 (4), 257–266.
Ryan, W., Lamb, B., Robinson, E., 1984. An atmospheric tracer investigation of transport and dispersion around a large, isolated hill and day-night transition periods. Atmos. Environ. 18, 2003–2021.
Sanderse, B., van der Pijl, S.P., Koren, B., 2011. Review of computational fluid dynamics for wind turbine wake aerodynamics. Wind Energy 14 (7), 799–819.
Schatzmann, M., Rafailidis, S., Pavageau, M., 1997. Some remarks on the validation of small-scale dispersion models with field and laboratory data. J. Wind Eng. Ind. Aerodyn. 67–68, 885–893.
Schatzmann, M., Leitl, B., 2011. Issues with validation of urban flow and dispersion CFD models. J. Wind Eng. Ind. Aerodyn. 99 (4), 169–186.
Schlünzen, K.H., Grawe, D., Bohnenstengel, S.I., Schlüter, I., Koppmann, R., 2011. Joint modelling of obstacle induced and mesoscale changes – current limits and challenges. J. Wind Eng. Ind. Aerodyn. 99, 217–225.
Shih, T.H., Liou, W.W., Shabbir, A., Zhu, J., 1995. A new k–ε eddy-viscosity model for high Reynolds number turbulent flows – model development and validation. Comput. Fluids 24 (3), 227–238.
Silva Lopes, A., JMLM, Palma, Castro, F.A., 2007. Simulation of the Askervein flow. Part 2: large-eddy simulations. Bound.-Layer Meteorol. 125, 85–108.
Stathopoulos, T., 2002. The numerical wind tunnel for industrial aerodynamics: real or virtual in the new millennium? Wind Struct. 5 (2–4), 193–208.
Stathopoulos, T., 1997. Computational wind engineering: past achievements and future challenges. J. Wind Eng. Ind. Aerodyn. 67–68, 509–532.
Stathopoulos, T., 2006. Pedestrian level winds and outdoor human comfort. J. Wind Eng. Ind. Aerodyn. 94 (11), 769–780.
Tamura, T., Cao, S., Okuno, A., 2007. LES study of turbulent boundary layer over a smooth and a rough 2D hill model. Flow Turbul. Combust. 79, 405–432.
Taylor, P.A., Gent, P.R., 1974. A model of atmospheric boundary-layer flow above an isolated two-dimensional "hill": an example of flow above 'gentle topography'. Bound.-Layer Meteorol. 7, 349–362.
Taylor, P.A., Walmsley, J.L., Salmon, J.R., 1983. A simple model of neutrally stratified boundary-layer flow over real terrain incorporating wavenumber-dependent scaling. Bound.-Lay. Meteorol. 26, 169–189.
Taylor, P.A., Teunissen, H.W., 1983. Askervein '82: Report on the September/October 1982 Experiment to Study Boundary Layer Flow Over Askervein, South Uist. Atmospheric Environment Service, Downsview, Ontario (Report MSRB-83-8).
Taylor, P.A., Teunissen, H.W., 1985. The Askervein Hill Project: Report on the September/October 1983 Main Field Experiment. Atmospheric Environment Service, Downsview, Ontario (Report MSRB-84-86).
Taylor, P.A., Teunissen, H.W., 1987. The Askervein hill project: overview and background data. Bound.-Layer Meteorol. 39 (1–2), 15–39.
Tominaga, Y., Stathopoulos, T., 2007. Turbulent Schmidt numbers for CFD analysis with various types of flowfield. Atmos. Environ. 41 (37), 8091–8099.
Tominaga, Y., Mochida, A., Yoshie, R., Kataoka, H., Nozu, T., Yoshikawa, M., Shirasawa, T., 2008. AIJ guidelines for practical applications of CFD to pedestrian wind environment around buildings. J. Wind Eng. Ind. Aerodyn. 96 (10–11), 1749–1761.
Tominaga, Y., Okaze, T., Mochida, A., 2011. CFD modeling of snowdrift around a building: an overview of models and evaluation of a new approach. Build. Environ. 46 (4), 899–910.
Tominaga, Y., Stathopoulos, T., 2013. CFD simulation of near-field pollutant dispersion in the urban environment: a review of current modelling techniques. Atmos. Environ. 79, 716–730.
Toparlar, Y., Blocken, B., Vos, P., van Heijst, G.J.F., Janssen, W.D., van Hooff, T., Montazeri, H., Timmermans, H.J.P., 2015. CFD simulation and validation of urban microclimate: a case study for Bergpolder Zuid, Rotterdam. Build. Environ. 83, 79–90.
Undheim, O., Andersson, H.I., Berge, E., 2006. Non-linear, microscale modelling of the flow over Askervein hill. Bound.-Layer Meteorol. 120, 477–495.
Van der Hoven, I., 1957. Power spectrum of horizontal wind speed in the frequency ragen from 0.0007–900 cycles per hour. J. Meteorol. 14, 160–164.
van Hooff, T., Blocken, B., 2010a. Coupled urban wind flow and indoor natural ventilation modelling on a high-resolution grid: a case study for the Amsterdam ArenA stadium. Environ. Model. Softw. 25 (1), 51–65.
van Hooff, T., Blocken, B., 2010b. On the effect of wind direction and urban surroundings on natural ventilation of a large semi-enclosed stadium. Comput. Fluids 39, 1146–1155.
van Hooff, T., Blocken, B., Aanen, L., Bronsema, B., 2011a. A venturi-shaped roof for wind-induced natural ventilation of buildings: wind tunnel and CFD evaluation of different design configurations. Build. Environ. 46 (9), 1797–1807.
van Hooff, T., Blocken, B., van Harten, M., 2011b. 3D CFD simulations of wind flow and wind-driven rain shelter in sports stadia: influence of stadium geometry. Build. Environ. 46 (1), 22–37.
Wakes, S.J., Maegli, T., Dickinson, K.J., Hilton, M.J., 2010. Numerical modelling of wind flow over a complex topography. Environ. Model. Softw. 25 (2), 237–247.
Walmsley, J.L., Salmon, J.R., Taylor, P.A., 1982. On the application of a model of boundary-layer flow over low hills to real terrain. Bound.-Layer Meteorol. 23, 17–46.
Wieringa, J., 1992. Updating the Davenport roughness classification. J. Wind Eng. Ind. Aerodyn. 41–44, 357–368.
Wood, N., 2000. Wind flow over complex terrain: a historical perspective and the prospect for large-eddy modelling. Bound.-Layer Meteorol. 96, 11–32.
Yamada, T., Koike, K., 2011. Downscaling mesoscale meteorological models for computational wind engineering applications. J. Wind Eng. Ind. Aerodyn. 99, 199–216.
Yang, Y., Gu, M., Chen, S., Jin, X., 2009. New inflow boundary conditions for modelling the neutral equilibrium atmospheric boundary layer in computational wind engineering. J. Wind Eng. Ind. Aerodyn. 97 (2), 88–95.
Yoshie, R., Mochida, A., Tominaga, Y., Kataoka, H., Harimoto, K., Nozu, T., Shirasawa, T., 2007. Cooperative project for CFD prediction of pedestrian wind environment in the Architectural Institute of Japan. J. Wind Eng. Ind. Aerodyn. 95 (9–11), 1551–1578.